8-1-1991

Liquid Phase Electrochemistry at Ultralow Temperatures

Royce W. Murray
University of North Carolina at Chapel Hill, rwm@email.unc.edu

Stanton Ching
Connecticut College, sschi@conncoll.edu

John T. McDevitt
University of Texas at Austin, mcdevitt@mial.utexas.edu

Stephen R. Peck

Recommended Citation
Ching, S., McDevitt, J. T., Peck, S. R., & Murray, R. W. Liquid phase electrochemistry at ultralow temperatures. *J. Electrochem. Soc.* ***1991**, 138, 2308-2315.*

Liquid Phase Electrochemistry at Ultralow Temperatures

Stanton Ching,[1] John T. McDevitt,[2] Stephen R. Peck, and Royce W. Murray*

Kenan Laboratories of Chemistry, University of North Carolina, Chapel Hill, North Carolina 27599-3290

ABSTRACT

Fluid electrolyte solutions based on mixtures of butyronitrile (PrCN) and ethyl chloride (EtCl) with Bu_4NPF_6 or Bu_4NClO_4 as electrolyte freeze below −180°C and provide excellent media for cryogenic electrochemical experiments. A 1:2 mixture of PrCN and EtCl exhibits the best combination of freezing point and ionic conductivity for ultralow temperature electrochemistry. Diffusion coefficients for bis(pentamethylcyclopentadienyl) iron (Cp^*_2Fe) are measurable by potential step chronoamperometry down to −160°C using a conventionally sized electrode, but the resistivity of the solvent mixture is such that potential sweep voltammetry benefits from the use of microdisk (10 and 25 μm diam Pt) or microband (0.2 μm wide Au) electrodes. Voltammetry at a chemically modified electrode down to −170°C is presented for the case of thin films of poly-$[Os(bpy)_2(vpy)_2][PF_6]_2$.

Interest in low-temperature electrochemistry (1-6) is traditionally tied to investigations of the kinetics of heterogeneous electron transfer reactions (7-11) and electrochemically induced homogeneous processes (2-6, 12-19) that otherwise, at ambient temperature, occur too rapidly. Such research is dependent upon fluid electrolyte systems with suitable low-temperature limits. Numerous organic solvents are available for electrochemistry down to, and slightly below, the temperature of a dry ice/acetone bath, −78°C. Butyronitrile (PrCN) is an excellent low-temperature medium; voltammetry in it to −135°C has been reported (14). Low-temperature electrochemistry has also been performed in frozen glass solids (20-25), and with the solid (20, 24) eutectic $HClO_4 \cdot 5H_2O$.

We recently (26) described a new cryogenic medium that extends the lower temperature limit of electrochemical voltammetry in liquids. Our interest in this subject stems from a desire to investigate the electron transfer properties and double-layer capacitance behavior of high-temperature superconductor electrodes in their superconducting state. Tremendous advances in the synthesis of high-temperature superconductors have pushed superconducting critical temperatures (T_c) above that of liquid nitrogen (−196°C) (27, 28). There are no reports on electrochemistry at these new materials in fluid electrolytes at temperatures below their T_c values, but interesting electrochemical effects have been observed at T_c in experiments using solid electrolytes (29-31). Use of a suitably low temperature fluid electrolyte would improve contact to the superconducting electrode interface (as compared to solid-solid contacts) and could potentially provide access to a greater range of electrochemical reactions and experimental techniques to study the electrochemistry of superconductor electrodes such as $YBa_2Cu_3O_7$ (T_c = −180°C), $Bi_2Sr_2Ca_2Cu_3O_{10}$ (T_c = −163°C), and $Tl_2Ba_2Ca_2Cu_3O_{10}$ (T_c = −148°) in their superconducting states. These materials may have electronic properties as electrodes unlike any previously investigated. We have already reported some of our work, so far carried out above T_c (32-34), with electrodes fabricated from the superconductor ceramic materials.

Experimental

Chemicals.—Butyronitrile and propionitrile (Aldrich) were distilled from CaH_2, and acetonitrile (Burdick and Jackson UV Spectra quality) was stored over 4 A molecular sieves. Ethyl chloride (EtCl, Linde) was condensed from a gas cylinder into a Schlenk-type storage tube over 4 A molecular sieves and kept at room temperature (vapor pressure *ca.* 1.5 atm). The electrolyte salts Bu_4NPF_6 and Bu_4NClO_4 (Fluka), bis(pentamethylcyclopentadienyl)iron, Cp^*_2Fe, Strem), and 7,7,8,8-tetracyanoquinodimethane (TCNQ, Aldrich) were used as received.

Low-temperature apparatus.—The low-temperature electrochemical cell consists of an outer, evacuated jacket and an inner jacket with feed-throughs for the coolant, which was a regulated flow of cold, dry nitrogen gas passed through coils of copper tubing immersed in liquid nitrogen. Temperatures were measured with calibrated K and T-type (Omega) thermocouples that were mounted as close as possible to the working electrode.

Solidification temperature determinations.—Solidification temperatures were determined, in the absence of added electrolyte, from changes in solution viscosity as detected by agitation of a wire thermocouple mounted on a glass rod. This method was checked using solvents of known freezing points and deemed reliable to within ±3°. Solidification temperatures of electrolyte-containing solvent systems were also determined by cyclic voltammetry. Background charging currents at a 0.5 mm diam Pt disk electrode resulting from ±0.3 V (*vs.* Ag wire) potential sweeps at 100 mV/s were monitored as the solution was slowly cooled. The solidification temperature was recorded as that for which the charging current suddenly decayed to near zero. Some precipitation of electrolyte was often observed at low temperatures, but this did not appear to adversely affect the charging measurements since the viscosity and voltammetric data were in good agreement.

Ethyl chloride (bp = +12°C) was handled at −78°C (dry ice/acetone bath). Mixtures of PrCN and EtCl with supporting electrolyte were prepared by dissolving the electrolyte in a measured volume of PrCN at room temperature, cooling the solution to approximately 0°C, and adding the desired amount of ethyl chloride precooled at −78°C using a calibrated pipette.

Resistivity measurements.—Solution resistivities were measured using an Industrial Instruments ac conductivity bridge (Cedar Grove, NJ) in the double-jacketed electrochemical cell described above, with two parallel (*ca.* 1 mm, spacing), platinized 1 cm^2 Pt sheets. The conductivity cell constant was calibrated with 0.100*M* aqueous KCl at 25°C (35). A bridge frequency of 10^3 Hz was used when the solution resistance was less than 10^4 Ω and 10 Hz when this value was exceeded. In selected cases, low-temperature solution resistivity was also measured (with satisfactory agreement) by ac impedance using a Solartron 1255 Frequency Analyzer and a 1286 Electrochemical Interface.

Electrochemistry.—Potential step chronoamperometry was carried out with a PAR 173 Potentiostat/Galvanostat and cyclic voltammetry with a potentiostat and waveform generator of local construction. A conventional, three-electrode configuration was used with Pt disk or microdisk (Pt microwire sealed in glass) or Au microband (see below) working electrode, Pt wire auxiliary electrode, and Ag wire quasi reference electrode. No iR_{uncomp} feedback compensation was employed.

At the 0.5 mm diam "macroelectrode," diffusion coefficients (D) of redox solutes were evaluated by potential step

* Electrochemical Society Active Member.
[1] Present address: Department of Chemistry, Connecticut College, New London, Connecticut 06320-4196.
[2] Present address: Department of Chemistry, University of Texas at Austin, Austin, Texas 78712-1167.

chronoamperometric, i *vs.* $t^{-1/2}$ plots according to the Cottrell equation

$$i = \frac{nFAD^{1/2}C^*}{(\pi t)^{1/2}} \quad [1]$$

where A = electrode area and C^* = redox solute concentration (mol/cm^3). At microdisk electrodes, D was calculated from the plateau steady-state currents of voltammograms from (36, 37)

$$i = 4nFrDC^* \quad [2]$$

in which r is the microdisk radius.

Gold microbands were fabricated from 0.2 μm films, on 0.025 in. polished Al_2O_3 wafers (Materials Research Corporation, Orangeburg, NY), made by undercoating with 0.02 μm Cr followed by Au vapor deposition onto all sides and edges. The wafers were cut into *ca.* 2.5 × 0.6 cm rectangles, polished to remove Au from the edges, and sandwiched between two glass slides with either Torrseal (Varian) or Epon 828 Epoxy (Shell, metaphenylenediamine curing agent, 13% by weight) sealant. The Epon epoxy was prone to delamination upon prolonged exposure to halocarbon solvents. One end of the wafer was left exposed to allow electrical contacts to the two Au films; after polishing the other end with 600 grit sandpaper, two 0.2 μm Au microbands were exposed as illustrated in Fig. 1a.

Microbands, unlike microdisks, do not yield true steady-state current plateaus, but at sufficiently small potential scan rates a pseudo-steady state is approached as illustrated in the example (room temperature) voltammogram in Fig. 1b. The microband relation (37-39) used is

$$i = \frac{\pi nFLDC^*}{\ln(8DRT/nFvW)} \quad [3]$$

in which L and W are length (typically 0.4-0.8 cm) and width (2.0×10^{-5} cm) of the microband, respectively, and experiment time has been replaced with RT/nFv where v is potential scan rate (V/s). For the voltammogram in Fig. 1b, the microband equation predicts (using a microdisk-measured $D_{TCNQ} = 1.53 \times 10^{-5}$ cm^2/s and the nominal 0.6 cm length and 0.2 μm width) a pseudo-plateau current of 417 nA which is in (typical) pair agreement with the observed 360 nA. (We observed that pseudo-steady-state currents at freshly fabricated microbands are sometimes, initially, more than 10-fold larger than anticipated, but within a day or so after fabrication, the current settles to a value near the theoretical prediction. Such behavior may be due to a mechanical relaxation of gaps between the epoxy sealant and the Au film created during polishing.)

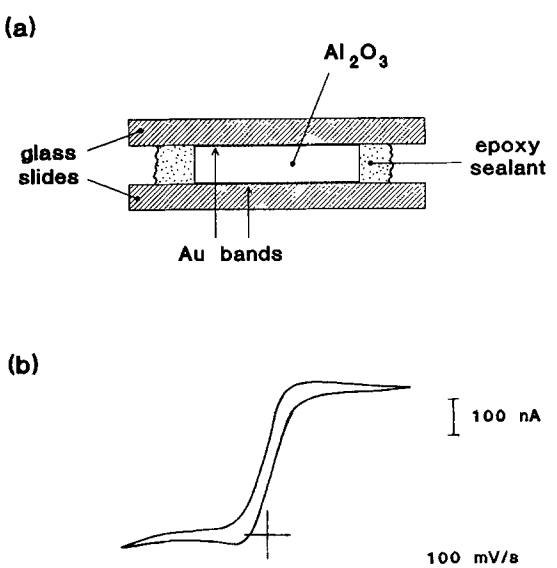

Fig. 1. (a) A schematic end-on view of a 0.2 μm Au microband electrode. The Au film/glass slide junction is sealed with epoxy and the Au film/Al_2O_3 wafer junction is anchored with a thin layer (0.025 μm) of Cr. (b) A sample cyclic voltammogram of the $TCNQ^{0/-1}$ couple (1 mM) in CH_3CN with 0.1*M* Bu_4NPF_6. The band dimensions are L = 0.6 cm and w = 0.2 μm.

Table I. Physical properties of nitrile and halogenated solvents (41).

Solvent	mp (°C)	ε (*T*, °C)	η (*T*, °C) (Centipoise)	Comments
Acetonitrile (MeCN)	−46	37.5 (20)	0.375 (15)	
Propionitrile (EtCN)	−92	27.2 (20)	0.454 (15)	
Butyronitrile (PrCN)	−112	20.3 (21)	0.624 (15)	
EtCl	−138	9.45 (20)	0.279 (10)	bp = +12°C
EtBr	−119	9.39 (20)	0.418 (15)	
2-Chlorobutane	−131	7.09 (30)	0.439 (15)	Racemic
$CHClF_2$	−160	6.11 (24)	0.23 (25)	bp = −41°C
$CHCl_2F$	−135	5.34 (28)	0.34 (25)	bp = +9°C
NF_3	−207	—	—	bp = −129°C
CH_2Cl_2	−97	9.08 (20)	0.45 (15)	

The Pt disk macroelectrodes were chemically modified with electropolymerized films of poly-$[Os(bpy)_2(vpy)_2][PF_6]_2$ (bpy = 2,2′-bipyridine; vpy = 4-vinylpyridine) as described previously (40). Film coverages in mol/cm^2 were determined from the electrochemical charge under the Os(II/III) voltammetric wave. An average monolayer coverage is taken as 1.3×10^{-10} mol/cm^2.

Results and Discussion

Low-temperature solvent systems.—Vital characteristics of an electrochemically useful low-temperature solvent system include low freezing or solidification temperature, low-temperature dissolution of electrolyte and redox solutes, and adequate electrolyte dissociation and ion mobility as reflected in the solution ionic conductivity. We selected a strategy of examining combinations of low-melting liquids (or condensable gases) with relatively high dielectric constants and low-viscosities that might generate low-freezing eutectic mixtures (41) or glasses. Butyronitrile (PrCN) was an attractive component, having an unusually large dielectric constant and a relatively low melting point. Small halogenated hydrocarbons have low melting points and lower but still significant dielectric constants. Table I gives known physical properties of some such materials.

Combining PrCN with halocarbons generally produces solvent systems which dissolve tetrabutylammonium salts to some extent and solidify between −160°C and −180°C. Mixing different halocarbons was less successful, giving solutions with poor dissolving powers. Admixtures with more than two components typically led to only minor improvements. Nitrogen trifluoride has an attractively low melting point, but we were unable to find dissoluble electrolytes and its −129°C boiling point makes NF_3 inconvenient to handle.

Mixtures of PrCN and EtCl were found to have superior low-temperature fluid electrolyte characteristics, shown in the solidification temperature diagrams in Fig. 2. Without dissolved electrolyte (○), a broad solidification minimum at *ca.* 1:1 PrCN:EtCl was observed near −180°C. Adding (△) 0.1-0.2*M* Bu_4NPF_6 electrolyte (or Bu_4NClO_4) caused two major changes: PrCN and EtCl individually display substantial solidification temperature depressions and the curve minimum remains close to −180°C but broadens considerably (1:1-1:2 PrCN:EtCl) and seems to shift toward greater percentages of EtCl. The former effect can be reasonably attributed to changes in colligative properties brought on by the dissolved electrolyte salt. We note that whether the solidification detected in the mixtures is caused by true freezing or by solvent glassing is unknown, so the cause of the Fig. 2 broadening is similarly obscure at this time.

Another important feature of a low-temperature electrochemical fluid is its ionic conductivity. Specific solution resistances (ρ) of several electrolyte solutions are reported

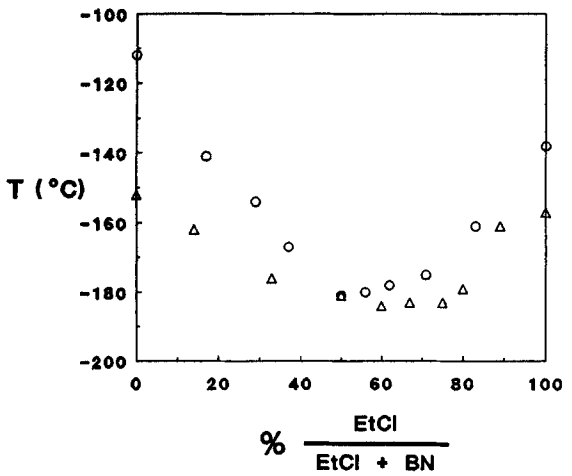

Fig. 2. Compositional phase diagrams for the PrCN:EtCl solvent system. Circles represent solidification temperatures obtained for solutions without supporting electrolyte and triangles represent data for 0.2M Bu_4NPF_6 solutions.

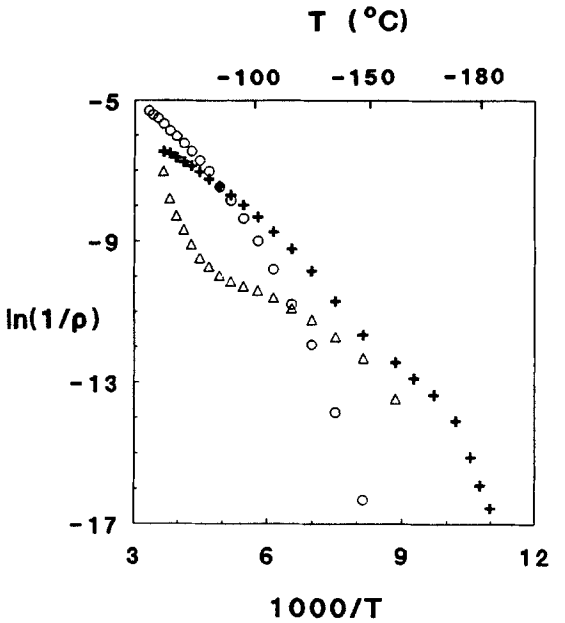

Fig. 3. Arrhenius plots for the ionic conductivity of 0.2M Bu_4NPF_6 liquid/electrolyte solutions neglecting the effects of electrolyte precipitation for: PrCN (○), EtCl (△), and 1:2 PrCN:EtCl (+).

in Table II as are activation energies for ion transport (42) obtained from Arrhenius plots ln(1/ρ) *vs.* 1/*T*, see Fig. 3.[3] Some of the distortions observed in Fig. 3 are obviously associated with electrolyte precipitation, such as the sharp decline in the EtCl conductivity data below 0°C. Some electrolyte precipitation is typical at low temperatures and is more noticeable in solutions with larger portions of EtCl. The amount of precipitation was judged, relative to the dissolved total, to be most substantial in the pure alkyl halide solvents and a less serious problem in the nitrile, mixed PrCN:EtBr and PrCN:EtCl solvents. The E_a values in Table II are high-temperature limits, being based on data at temperatures above those at which any significant precipitation was noticed.

The resistivity results in Table II and Fig. 3 reflect the combined degree of electrolyte dissociation, ion mobilities, and losses in concentration due to precipitation. Electrolyte dissociation is promoted by large solvent dielectric constant and ion mobility (through Stokes' law) by low solvent viscosity. Thus, at all temperatures, electrolyte solution resistances in nitriles (alone) increase in the order ρ(MeCN) < ρ(EtCN) < ρ(PrCN), which is in the same order as increasing viscosity and decreasing dielectric constant (Table I). The dielectric constants for EtBr and EtCl are nearly the same, but ρ(EtBr) > ρ(EtCl), which shows more directly the importance of viscosity since η(EtBr) > η(EtCl). Other publications have also stressed the role of viscosity in low-temperature solution resistance (1, 42).

The effects of solvent viscosity are also apparent in the solvent mixtures, where electrolyte precipitation is also less severe. For example, ρ(1:1 PrCN:EtCl) < ρ(1:1 PrCN:EtBr) at −160°C, and ρ(PrCN:EtCl) decreases with greater proportions of EtCl. This trend is not as expected from dielectric constant but follows that for viscosity.[4] The E_a for ion transport in PrCN:EtCl mixtures also falls with increasing proportion of EtCl consistent with lowering of viscosity. Another important point evident in Table II and Fig. 3 is that the solution resistance of the solvent mixture at the lower temperatures is significantly less than that of either individual solvent component, reflecting the importance of considering the dielectric constant and solvent viscosity. The higher dielectric component (PrCN) promotes electrolyte dissociation and the lower viscosity component (EtCl) facilitates ionic mobility to enhance product of charge carrier population and mobility.

Figure 3 also shows, for the 1:2 PrCN:EtCl mixture, that the solution conductivity falls much more rapidly with decreasing temperature below −170°C. This change in behavior is observed to some extent in all the PrCN:EtCl mixtures and is exacerbated at higher fractions of EtCl. The phenomenon in part may reflect electrolyte precipitation but is probably also related to the onset of solvent solidification or glassing; the details are unknown at this point.

We examined several other tetrabutylammonium electrolytes but none proved preferable to Bu_4NPF_6 and Bu_4NClO_4, although Hx_4NClO_4 is not very different. The resistivities of alkylammonium salt solutions has been reported (44) as being less for short alkyl chains. However, Table II shows a much larger resistivity for Et_4NClO_4 in 1:1 PrCN:EtCl, probably because it is more prone to precipitation.

Electrochemistry in 1:2 PrCN:EtCl.—The low-temperature potential window in 0.2M Bu_4NPF_6 1:2 PrCN:EtCl solvent mixture is quite large at a 25 μm diam Pt microdisk electrode (Fig. 4), expanding from *ca.* +2.0 to −1.8 V at −78°C to *ca.* ±3.0 V at −160°C. This change is consistent with slow kinetic rates for background discharge of solvent (or electrolyte), generating larger reaction overpotentials at lowered temperature. Similar effects have been observed by Evans and co-workers (43).

Table II makes it clear that while 0.2M Bu_4NPF_6 1:2 PrCN:EtCl is a low-temperature electrolyte solution, it is, nonetheless, a very resistive solvent and thus demands care in experiment design. Solvent resistance effects can severely distort potential scan voltammograms at macrosized working electrodes, whereas microelectrodes are more tolerant (45) of resistive media, because of the small currents that flow. For example, voltammograms of Cp^*_2Fe at electrodes with diameters greater than 50 μm exhibit severe uncompensated resistance distortion below *ca.* −100°C, but with 10 and 25 μm diam microdisks could be recorded down to −150°C, as illustrated in Fig. 5. At the lowest temperatures, the experiment is degraded by a combination of very small currents and a marginal ratio of current for Cp^*_2Fe oxidation to double-layer charging (electrode capacitance) as the potential is scanned. Figure 5 reveals that decreases in the diffusion coefficient of Cp^*_2Fe at the lowered temperatures are greater than any that occur in the double-layer capacitance. The potential scan rate can of course be lowered to improve the ratio of faradaic/charging current. Values for $D_{Cp^*_2Fe}$ at low temperatures can be evaluated (Eq. [2]) from the radial diffusion-limited plateau currents at 10 μm diam microdisks, and as seen in Table III, they change by 400-fold between −20 and −150°C.

[3] Modeling ion conduction in solution as an activated ion-hopping process leads to an Arrhenius-type expression $\lambda_i = ze_oFL^2/6h \exp -E_A/RT$ where the pre-exponential terms comprise the limiting ionic conductance, z and e_o are the ionic and electronic charges, and E_A is the barrier height to hops of length L.

[4] We assume that both the dielectric constant and viscosity of the mixtures decrease at −160°C with increasing proportion of EtCl.

Table II. Resistivity measurements for low-temperature solvent systems.

Solvent system (Electrolyte)[a]	T[b] (°C)	ρ (K, Ωcm)	fp[c] (°C)	E_a[d] (kcal/mol)	Precipitation
MeCN	0	0.12	−55–−60	1.8(3)	−45
(0.2*M* Bu_4NPF_6)	−40	0.21			
EtCN	0	0.17	−105–−110	2.1(4)	−90
(0.2*M* Bu_4NPF_6)	−40	0.32			
	−80	0.93			
PrCN	0	0.30	−150	2.7(7)	−100
(0.2*M* Bu_4NPF_6)	−40	0.64			
	−80	2.6			
	−120	49			
EtCl	0	1.1	−160	—	0
(0.2*M* Bu_4NPF_6)	−40	8.9			
	−80	25			
	−120	54			
EtBr	0	1.7	−130	2.3(1)	−20
(0.2*M* Bu_4NPF_6)	−40	20			
	−80	195			
	−120	815			
PrCN:EtBr 1:1	0	0.40	−175	2.1(2)	−70
(0.2*M* Bu_4NPF_6)	−40	0.78			
	−80	2.3			
	−120	18			
	−160	768			
PrCN:EtCl 1:1	0	0.41	−178	1.7(1)	−50
(0.2*M* Bu_4NPF_6)	−40	0.68			
	−80	1.8			
	−120	11			
	−160	459			
PrCN:EtCl 1:2	0	0.64	−182	1.4(1)	−50
(0.2*M* Bu_4NPF_6	−40	0.97			
	−80	2.2			
	−120	10			
	−160	253			
PrCN:EtCl 1:1	0	0.59	−178	1.8(5)	−80
(0.2*M* Bu_4NClO_4)	−40	0.98			
	−80	2.5			
	−120	16			
	−160	618			
PrCN:EtCl 1:2	0	0.65	−182	1.5(6)	−60
(0.2*M* Bu_4NClO_4)	−40	1.0			
	−80	2.4			
	−120	11			
	−160	314			
PrCN:EtCl 1:1	0	4.4	−161	—	Significant
(0.2*M* Et_4NClO_4)	−40	12.2			at 0.
	−80	46			
	−120	309			
	−160	18,300			
PrCN:EtCl 1:1	0	0.58	−175	1.85(3)	−60
(0.2*M* Hx_4NClO_4)	−40	1.0			
	−80	2.6			
	−120	15			
	−160	600			

[a] Values represent concentrations calculated for room temperature. The volume of PrCN is measured at room temperature and the volume of EtCl is measured at −78°C.
[b] Representative data are shown. Measurements were taken every 10° from room temperature to the solidification point or from 0° to the solidification point if EtCl was used.
[c] Temperatures at which the last resistance measurement was recorded before the values fell off scale.
[d] Data were used only if no precipitate was observed, so the results represent higher temperature data.

Voltammograms at the 25 μm diam microdisk (Fig. 5) show a change suggestive of linear diffusion at −140°C and lower, which is quantitatively expected since radial diffusion is less quickly attained at the larger electrode. The 0.2 V peak splitting in the −150°C voltammogram is about 100-fold larger than that anticipated for an iR_{uncomp} effect using the measured $D_{Cp^*_2Fe}$ (Table III chronoamperometry data) and solvent ρ (Fig. 3) values in the relation

$$iR_{uncomp} = \frac{1.5 \times 10^6 n^{3/2} r v^{1/2} D^{1/2} c^* \rho}{T^{1/2}} \quad [4]$$

which can be derived by combining the linear diffusion Randles-Sevcik equation (46) with the relationship for resistance at a hemisphere, $R = \rho/4r$. The peak splitting may reflect some ferricenium salt precipitation (45) or slow charge transfer for the $Cp^*_2Fe^{0/+}$ redox couple at low temperatures; this has not been studied further.

The voltammetry in Fig. 5 illustrates that while well-defined cyclic voltammograms are obtained in the resistive 0.2*M* Bu_4NPF_6 1:2 PrCN:EtCl solvent mixture, the currents become distressingly small at the lowest temperatures. Such measurements are aided by the use of microband electrodes, which are extremely thin in one dimension but are relatively long in a second direction, thus providing an electrode whose overall surface area is considerably greater than that of a microdisk electrode (36). The advantage of this geometry is that fairly large (both radial and linear) voltammetric currents are generated while favorable iR_{uncomp} characteristics are retained. At slow potential scan rates, microband electrodes produce sigmoidal, pseudo-steady-state voltammograms by establishing hemicylindrical radial diffusion profiles over the length of the band. Microbands fabricated from commercially available thin (0.2 μm) Au films coated on Al_2O_3 substrates give larger currents in the low-temperature voltammetry of Cp^*_2Fe (Fig. 6), as expected. Recognizable waves can be distinguished to −160°C using the microband. Distortions in the waves at the lowest temperatures may be due to filming or slow charge transfer as noted above. These microbands are 5-fold wider than those employed in our previous report in which an even lower temperature limit was achieved (26).

Low-temperature electrochemistry was also accomplished with a 0.5 mm diam Pt disk, in this case using potential step chronoamperometry to measure diffusion

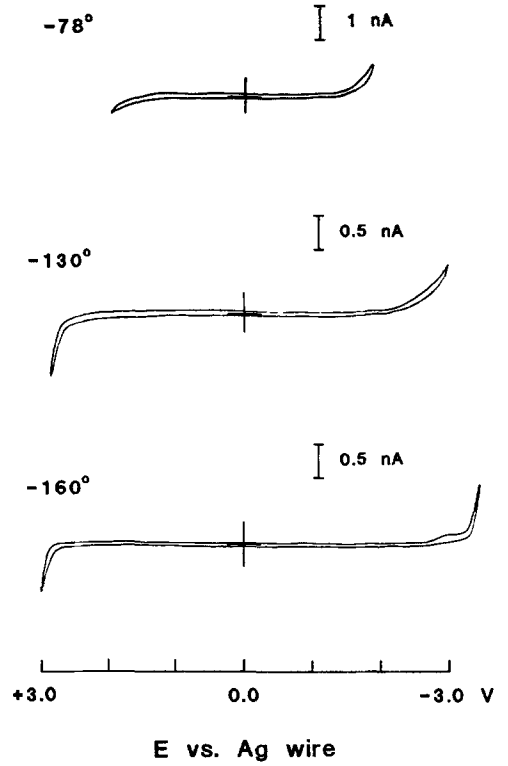

Fig. 4. Background cyclic voltammograms defining the potential limits of 0.2M Bu_4NPF_6 1:2 PrCN:EtCl at various temperatures. The voltammograms were recorded with a 25 μm diam Pt disk electrode at a scan rate of 100 mV/s.

coefficients of Cp^*_2Fe in 1:2 PrCN:EtCl solvent mixture. A large potential step (−0.5-+1.5 V *vs.* Ag wire) was applied to overcome iR_{uncomp} effects; this procedure generated linear i *vs.* $t^{-1/2}$ (Eq. [1]) plots for currents measured 3-4 s after applying the potential step.

Diffusion coefficients for Cp^*_2Fe from potential step chronoamperometry, microelectrode voltammetry, and microband voltammetry are summarized in Table III and given as Arrhenius plots in Fig. 7. D values at Pt macrodisks, microdisks, and Au microbands were determined from Eq. [1]-[3], respectively. Figure 7 shows that D values for Cp^*_2Fe from macrodisk chronoamperometry and microband voltammetry at low temperatures are quite comparable, as are apparent diffusional activation energies (2.1 and 2.3 kcal/mol, respectively). In contrast, lower results are obtained with microdisk experiments, notably below *ca.* −100°C. This microdisk difference is in the wrong direction for error due to not attaining purely radial diffusion conditions, which should manifest itself in a positive ln (D) *vs.* $1/T$ deviation (for radial diffusion, $D \alpha i$; for linear diffusion, $D \alpha i^2$). The quantitative inconsistency of the microdisk results is due to some experimental flaw which we could not identify. In any case, Table III shows that microband voltammetry and potential step chronoamperometry are suitable techniques for low-temperature electrochemistry. Microbands outperform microdisks with respect to producing larger currents while similarly controlling iR_{uncomp} distortions; potential step chronoamperometry is reliable provided a sufficient potential range is available for the large potential step needed to avoid iR_{uncomp} difficulties.

Table III. Diffusion coefficients of Cp^*_2Fe at variable temperatures.

	$D \times 10^8$ (cm²/s)		
T (°C)	Chronoamperometry[a]	Microdisk[b]	Microband[c]
0	723		
−20	482	438	
−40	317	283	
−60	244	170	
−80	180	95	
−100	95	40	103
−110	52	22	72
−120	36	11	44
−130	22	4.6	26
−140	10	1.2	16
−150	5.0	0.2	5.9
−160	3.1		3.0

[a] 0.5 mm diam Pt disk; Eq. [1].
[b] 10 μm diam Pt disk; Eq. [2].
[c] 0.2 μm × 0.6 cm Au band; Eq. [3] via iterations using i_{obsd} from cyclic voltammograms and beginning the calculations with D values from chronoamperometry.

Chemically modified electrodes (47) hold promise for electrochemical investigations at ultralow temperatures because of their special transport characteristics. Currents due to surface-confined electroactive compounds are not controlled by diffusion through the bulk solvent, so in principle, both the absolute value and the ratio of the faradaic current to capacitance currents should be independent of temperature. Furthermore, solubility of the electroactive species with increasing temperatures is no

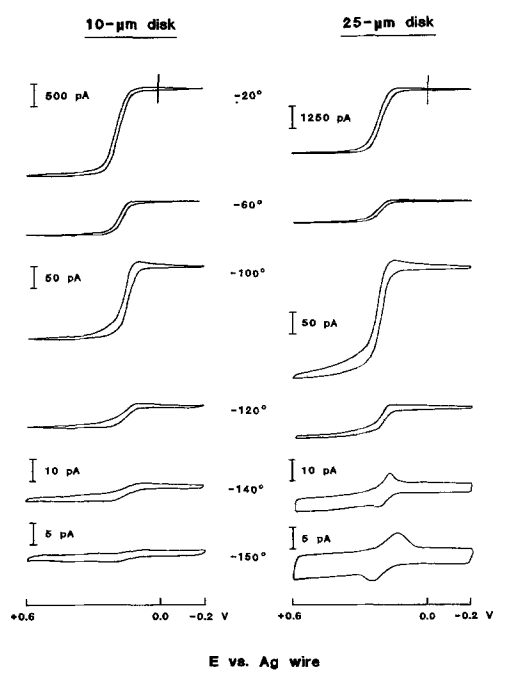

Fig. 5. Variable-temperature cyclic voltammograms (50 mV/s) recorded at 10 (left panel) and 25 μm (right panel) Pt microelectrodes for 2 mM Cp^*_2Fe in 0.2M Bu_4NPF_6 1:2 PrCN:EtCl.

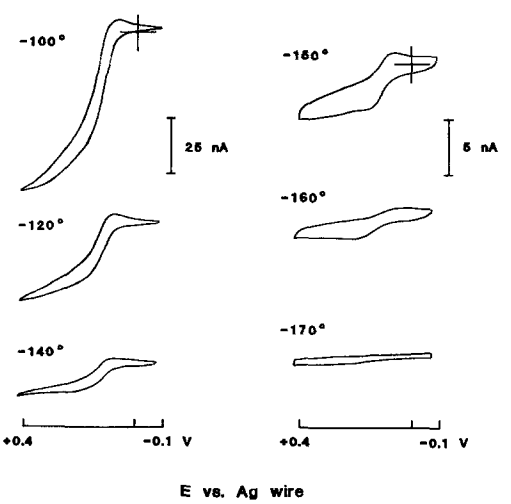

Fig. 6. Variable-temperature cyclic voltammograms for 2 mM Cp^*_2Fe recorded at 20 mV/s at a Au microband electrode ($w = 2 \times 10^{-5}$ cm; $L = 0.6$ cm) in 0.2M Bu_4NPF_6 1:2 PrCN:EtCl.

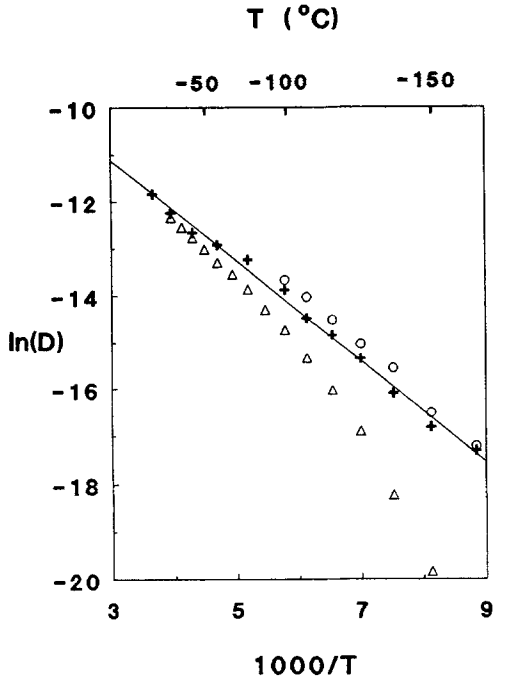

Fig. 7. Arrhenius plots of diffusion coefficient of Cp^*_2Fe (2 mM) in 1:2 0.2M Bu_4NPF_6 PrCN:EtCl. Diffusion coefficients were determined from chronoamperometry (+) at a 0.5 mm Pt disk, radial steady-state current measurements (△) at a 10 μm Pt microdisk, and pseudo-steady-state current measurements (○) at a 0.2 μm × 0.6 cm microband.

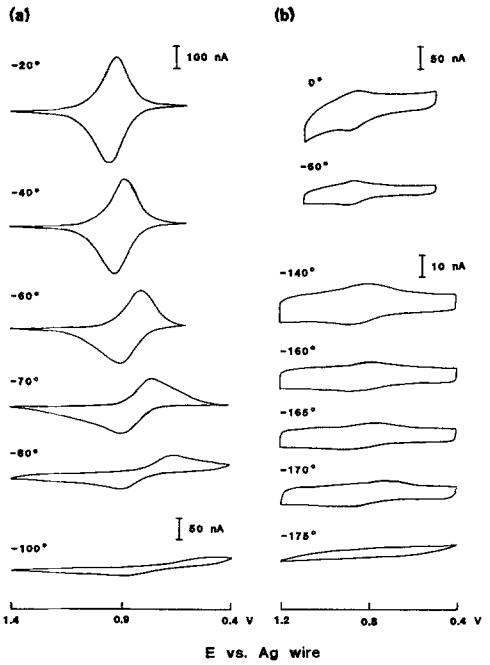

Fig. 8. Variable-temperature cyclic voltammograms (100 mV/s) of poly-$[Os(bpy)_2(vpy)_2][PF_6]$ films on 0.5 mm diam Pt disks in 0.2M Bu_4NPF_6 1:2 PrCN:EtCl: (a) for 10-monolayer film coverage, (b) for 1.4-monolayer coverage.

longer an issue and, if the quantity of surface-confined material, and thus the faradaic currents, is minimized, serious iR_{uncomp} effects can be avoided. A potential difficulty with many surface-confined materials, however, concerns rate-limiting diffusion (of electrons and counterions) within the film itself (48). This transport problem can be minimized by using very thin films. Indeed at low temperatures it can be more desirable to employ chemically modified macro-sized electrodes, in contrast to the theme of using micro-electrodes for low-temperature voltammetry of redox solutes, described above.

These features are illustrated with the Os(II/III) voltammetry from films of electrochemically polymerized poly-$[Os(bpy)_2(vpy)_2][PF_6]_2$, (bpy = 2,2′-bipyridine; vpy = 4-vinylpyridine), which has been well studied as to its redox characteristics (49-53).

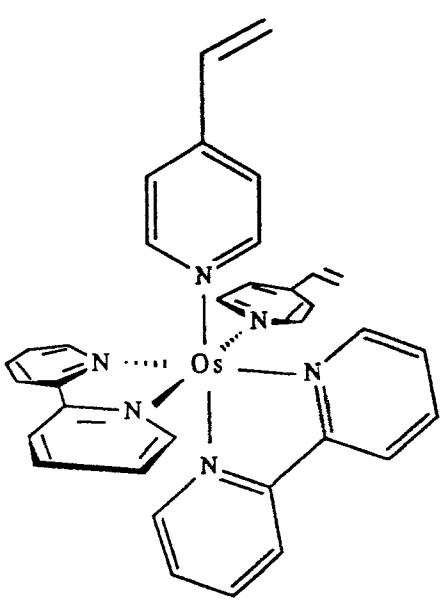

$[Os(bpy)_2(vpy)_2]^{2+}$

It has been demonstrated that both counterion and electron-hopping diffusion are substantially attenuated in this polymer system at low temperatures (52) and that lower temperatures have a greater influence on counterion motion. For this reason, films containing low (average 10 and 1) numbers of monolayers were deposited.

Variable-temperature voltammetry of two poly-$[Os(bpy)_2(vpy)_2]^{2+}$ films on 0.5 mm Pt disks, nominally 1.4 and 10 monolayers thick, is shown in Fig. 8. The two films exhibit nearly ideal peak separation ($\Delta E_p \approx 0$) at higher temperatures. However, for the 10-monolayer thick film (Fig. 8a) ΔE_p values increase significantly at temperatures below −60°C. At −100°C, the faradaic component of the voltammetric wave is barely recognizable. By contrast, the thinner poly-$[Os(bpy)_2(vpy)_2]^{2+}$ film ($\Gamma_T = 1.8 \times 10^{-10}$ mol/cm^2) is quite well behaved down to −160°C and is distorted but discernible at −170°C, Fig. 8b.

The 1.4 monolayer thick film probably does not coat the electrode in a uniform fashion. Instead, the film is likely to be made up of small clusters of oligomers scattered on the surface. Nonetheless, the charge-compensating counterions that are required to retain charge neutrality during the electron transfer to and from the Os complexes in these clusters need not penetrate into a thick polymer matrix to reach all the electroactive sites. Such will not be the case for the thicker film. Permeability measurements (53) on films 20 monolayers or thicker have shown that the electrode is more or less completely covered with polymer. Thus, counterion permeation through a large number of layers of electroactive sites is required in electrode reactions involving relatively thick films. This barrier to ion diffusion is likely to be accentuated as the amorphous polymer matrix becomes increasingly rigid at lower temperatures.

We interpret the qualitative features of the voltammograms in Fig. 8a then as reflecting a large iR_{uncomp} within the polymer matrix due to slow counterion transport in the thicker film. These experiments reveal that access to ultra-low-temperature voltammetry with surface-confined materials is possible and convenient, even with large electrodes, provided transport problems within the film itself can be resolved. There are numerous monolayer-attachment schemes in the chemically modified electrode literature that can potentially be exploited.

Finally, an example of slow charge transfer kinetics is found in low-temperature oxidative stripping of thin Ag

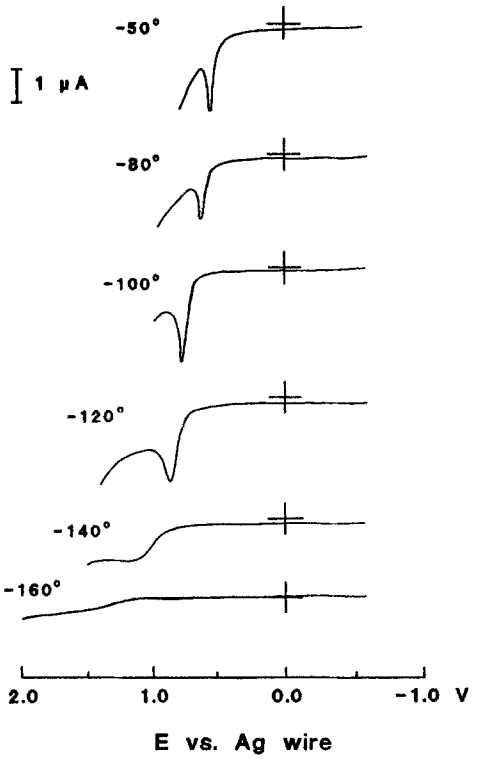

Fig. 9. Variable-temperature stripping voltammograms (100 mV/s) of Ag films which had been deposited on a 0.5 mm diam Pt electrode at room temperature from 0.1M Bu_4NPF_6 PrCN:EtCl solution saturated with silver acetate. Deposition times of 10 s were employed for films that were stripped at temperatures down to −80°C and 30 s for films stripped below this temperature.

metal films. Figure 9 shows the stripping of similar quantities of thin Ag metal films that were first electrochemically deposited on the Pt electrode from dilute Ag^+ solutions at room temperature, then cooled to lower temperatures at which the metal film was electrochemically oxidized. Each stripping curve represents a separate room temperature deposition cycle. The increasing shifts in the oxidation peak potential at lowered temperature represent larger and larger overpotentials for the oxidation reaction as the temperature is lowered. The shifts are much larger than accountable either from reference electrode variability or from iR_{uncomp} effects.

Summary

We have discovered a new fluid electrolyte system, 1:2 PrCN:EtCl with Bu_4NPF_6 or Bu_4NClO_4 supporting electrolyte, which is well suited for low-temperature electrochemistry. The application of this solvent system in chronoamperometry and cyclic voltammetric experiments with microelectrodes and chemically modified electrodes has produced results at temperatures lower than any previously reported in liquid media. A practical working limit in the range of −160–−170°C opens the possibility of conducting electrochemical experiments with some of the Bi- and Tl-based high-temperature superconductors, which is the ultimate goal of this research.

Acknowledgments

This research was funded in part by grants from the National Science Foundation and the Office of Naval Research. This work is part of a collaborative effort with G. T. Yee, Professor J. P. Collman, and Professor W. A. Little, Stanford University, to develop the methodologies needed for conducting electrochemical measurements at superconducting electrodes. We thank our collaborators for useful suggestions.

Manuscript submitted Dec. 26, 1990; revised manuscript received March 15, 1991.

The University of North Carolina assisted in meeting the publication costs of this article.

REFERENCES

1. R. P. Van Duyne and C. N. Reilley, *Anal. Chem.*, **44,** 142 (1972).
2. R. P. Van Duyne and C. N. Reilley, *ibid.*, **44,** 153 (1972).
3. R. P. Van Duyne and C. N. Reilley, *ibid.*, **44,** 158 (1972).
4. R. D. Grypa and J. T. Maloy, *This Journal,* **122,** 377 (1975).
5. R. D. Grypa and J. T. Maloy, *ibid.*, **122,** 509 (1975).
6. B. M. Bezilla, Jr., and J. T. Maloy, *ibid.*, **122,** 377 (1975).
7. B. E. Conway and M. Salomon, *J. Chem. Phys.*, **41,** 3169 (1964).
8. B. E. Conway and D. J. MacKinnon, *This Journal,* **116,** 1665 (1969).
9. R. Dietz and M. E. Peover, *Disc. Faraday Soc.*, **45,** 154 (1968).
10. G. J. Hoijtink, *Surf. Sci.*, **18,** 1 (1967).
11. T. Nagaoka and S. Okazaki, *J. Phys. Chem.*, **89,** 2340 (1985).
12. A. J. Klein and D. H. Evans, *J. Am. Chem. Soc.*, **101,** 757 (1979).
13. D. H. Evans and R. W. Busch, *ibid.*, **104,** 5057 (1982).
14. K. M. O'Connell and D. H. Evans, *ibid.*, **105,** 1473 (1983).
15. W. J. Bowyer and D. H. Evans, *J. Electroanal. Chem.*, **240,** 227 (1988).
16. W. J. Bowyer and D. H. Evans, *J. Org. Chem.*, **53,** 5234 (1988).
17. F. L. Wimmer, M. R. Snow, and A. M. Bond, *Inorg. Chem.*, **13,** 1617 (1974).
18. A. M. Bond, R. Colton, and J. J. Jackowski, *ibid.*, **14,** 274 (1975).
19. A. M. Bond, D. J. Darensbourg, E. Mocellin, and B. J. Stewart, *J. Am. Chem. Soc.*, **103,** 6827 (1981).
20. U. Stimming and W. Schmickler, *J. Electroanal. Chem.*, **150,** 125 (1983).
21. U. Frese and U. Stimming, *ibid.*, **198,** 409 (1986).
22. U. Frese, T. Iwasita, W. Schmickler, and U. Stimming, *J. Phys. Chem.*, **89,** 1059 (1985).
23. T. Dinan and U. Stimming, *J. Electroanal. Chem.*, **133,** 2662 (1986).
24. A. Matsunaga, K. Itoh, A. Fujishima, and K. Honda, *ibid.*, **205,** 343 (1986).
25. A. M. Bond, M. Fleischmann, and J. Robinson, *ibid.*, **180,** 257 (1984).
26. J. T. McDevitt, S. Ching, M. Sullivan, and R. W. Murray, *J. Am. Chem. Soc.*, **111,** 4528 (1989).
27. A. W. Sleight, *Science,* **242,** 1519 (1988).
28. T. V. Ramakrishnan and C. N. R. Rao, *J. Phys. Chem.*, **93,** 4414 (1989).
29. A. Pinkowski, J. Doneit, K. Juttner, W. J. Lorenz, Saemann-Ischenko, and M. Breiter, *Europhys. Lett.*, **9,** 269 (1989).
30. A. Pinkowski, J. Doneit, K. Juttner, W. J. Lorenz, Saemann-Ischenko, T. Zetterer, and M. Breiter, *Electrochim. Acta,* **34,** 1113 (1989).
31. A. Pinkowski, K. Juttner, and W. J. Lorenz, *J. Electroanal. Chem.*, **287,** 203 (1990).
32. J. T. McDevitt, M. Longmire, R. Gollmar, J. C. Jernigan, E. F. Dalton, R. L. McCarley, R. W. Murray, W. A. Little, G. T. Yee, M. J. Holcomb, J. E. Hutchinson, and J. P. Collman, *J. Electroanal. Chem.*, **243,** 465 (1988).
33. J. T. McDevitt, R. L. McCarley, E. F. Dalton, R. Gollmar, R. W. Murray, J. Collman, G. T. Yee, and W. A. Little, in "Chemistry of High-Temperature Superconductors II," D. L. Nelson and T. F. George, Editors, p. 207, ACS Symposium Series, American Chemical Society, Washington, DC (1988).
34. R. Gollmar, J. T. McDevitt, R. W. Murray, J. P. Collman, G. T. Yee, and W. A. Little, *This Journal,* **136,** 3696 (1989).
35. G. Jones and B. C. Bradshaw, *J. Am. Chem. Soc.*, **55,** 1781 (1933).
36. Y. Saito, *Rev. Polarogr.*, **15,** 178 (1968).
37. R. M. Wightman and D. O. Wipf, in "Electroanalytical Chemistry," Vol. 15, A. J. Bard, Editor, p. 267, Marcel Dekker, New York (1989).
38. K. R. Wehmeyer, M. R. Deakin, and R. M. Wightman, *Anal. Chem.*, **57,** 1913 (1985).
39. T. Varco Shea and A. J. Bard, *Anal. Chem.*, **59,** 2101 (1987).
40. J. M. Calvert, R. H. Schmehl, B. P. Sullivan, J. S. Facci, T. J. Meyer, and R. W. Murray, *Inorg. Chem.*, **22,** 2151 (1983).
41. (a) "Technique of Organic Chemistry," Vol. VII, A. Weissberger, Editor, Interscience, New York (1955);

(b) "Lange's Handbook of Chemistry," 13th ed., J. A. Dean, Editor, McGraw-Hill, New York (1985); (c) "Handbook of Organic Chemistry," J. A. Dean, Editor, McGraw-Hill, New York (1987).
42. S. B. Brummer and G. J. Hills, *Trans. Faraday Soc.*, **57,** 1816 (1961).
43. W. J. Bowyer, E. E. Engelman, and D. H. Evans, *J. Electroanal. Chem.*, **262,** 67 (1989).
44. H. O. House, E. Feng, and N. P. Peet, *J. Org. Chem.*, **36,** 2371 (1971).
45. L. Geng, A. G. Ewing, J. C. Jernigan, and R. W. Murray, *Anal. Chem.*, **58,** 852 (1986).
46. A. J. Bard and L. R. Faulkner, "Electrochemical Methods: Fundamentals and Applications, Chap. 6, John Wiley & Sons, New York (1980).
47. R. W. Murray, in "Electroanalytical Chemistry," Vol. 13, A. J. Bard, Editor, p. 191, Marcel Dekker, New York (1984).
48. C. P. Andrieux and J. M. Saveant, *J. Phys. Chem.*, **92,** 6761 (1988), and Ref. (1) and (2) therein.
49. C. E. D. Chidsey and R. W. Murray, *J. Phys. Chem.*, **90,** 1479 (1986).
50. J. C. Jernigan and R. W. Murray, *J. Am. Chem. Soc.*, **109,** 1738 (1987).
51. R. L. McCarley, R. E. Thomas, E. A. Irene, and R. W. Murray, *This Journal*, **137,** 1485 (1990).
52. J. C. Jernigan and R. W. Murray, *J. Phys. Chem.*, **91,** 2030 (1987).
53. C. R. Leidner and R. W. Murray, *J. Am. Chem. Soc.*, **106,** 1606 (1984).

On the Kinetics and Mechanism of Oxygen Reduction at Oxide Film-Covered Pt Electrodes in Acid Solutions

II. Electron Transfer Through the Oxide Film and Mechanism of the Reduction

A. Damjanovic

Allied Signal, Incorporated, Corporate Technology Center, Morristown, New Jersey 07960

ABSTRACT

The kinetics and mechanism of oxygen reduction at oxide film-covered Pt electrodes in acid solution is analyzed. Two linear E-log i regions are observed when it is ensured that the thickness of the oxide film for each E-log i point is the same. The kinetics in the high current density (cd) region is characterized by the Tafel slope of −120 mV. In the low cd region, the slope is −60 mV. The reaction order with respect to H_3O^+ is 1/2 and 1 in the high- and the low-cd region, respectively. Because of the observed fractional reaction order in the high-cd region, the kinetics in either cd region cannot be explained in terms of any classical, commonly used procedure in mechanistic analysis with a simple model of electrified interfaces. Currents at a constant potential in the cd region with the −120 mV slopes decrease exponentially with the thickness of the oxide film. In contrast, currents in the region with the −60 mV slope are invariant with thickness. Three models are used in mechanism analysis to account for the observed pH dependencies. The model of splitting the interfacial potential difference into two components, and the acid-base equilibria model can explain the observed pH dependencies. However, they do not account for the observed kinetic behavior with respect to the thickness of the oxide film. The model of the distribution of the unoccupied electron energy levels in solution and electron tunneling through the oxide film accounts both for the observed pH dependencies and for the dependence of the rates on oxide film thickness. With this model it is shown that the electron energy level in the ground state of the reacting complex increases 60 meV as pH increases one unit. This dependence of the electron energy levels on pH provides physical significance for the observed pH dependence and fractional reaction order with respect to H_3O^+.

It has been reported in *This Journal* that the kinetics of oxygen reduction (OR) at oxide film-covered Pt electrodes in acid solutions shows unusual behavior with respect to pH and the thickness of surface oxide films anodically formed prior to the measurements of the O_2 reduction rates (1). For a constant thickness of the film, two linear E-log i regions are seen (Fig. 1). At the low-cd end, they are close to −60 mV, *i.e.*, to $-2.3\ RT/F$, whereas at the high-cd end, they are close to −120 mV, *i.e.*, to $-2.3\ (2RT/F)$. At any constant cd and thickness of the oxide film, electrode potential against a pH-independent reference electrode decreases, in both cd regions, *ca.* 60 mV as pH values increase one unit, *i.e.*

$$\left[\frac{dE}{d\mathrm{pH}}\right]_{i,d} \approx -\frac{2.3RT}{F} \qquad [1]$$

While this pH dependence is compatible with the $(dE/d \log i)_{pH} \approx -2.3RT/F$ in the low-cd region, it cannot be reconciled on the basis of any simple model of electrode kinetics with the observed $dE/d \log i$ dependence of $-2.3\ (2RT/F)$ in the high-cd region.

Another feature of the kinetics is that the positions of the E-log i relations in the high-cd region with the −120 mV Tafel slopes depend strongly on the thickness of the oxide film. The rates of the OR at a given electrode potential decrease exponentially with film thickness (1). In contrast, the positions of the E-log i relations in the low region with the −60 mV Tafel slopes are essentially insensitive to the thickness of the oxide film. This is illustrated in Fig. 1 for an electrode which was for each point first reduced and then preanodized with 2×10^{-3} A cm^{-2} for either 10^2 or 10^4 s. With the previously published data (2, 3), the oxide film thickness for these two times of preanodization at this current density should approximately equal 7 and 8.5 Å, respectively.

In this paper, the pH dependencies in both cd regions are analyzed and an explanation is given for the dependence of the rates for OR on oxide film thickness in the high-cd region with the −120 mV Tafel slope, as well as for the independence of the rates on film thickness in the low-cd region with the −60 mV Tafel slope. A reaction path with its mechanisms is suggested that accounts for the observed kinetic parameters in both cd regions.

Kinetic Data

The kinetics of the OR in the high-cd region is described by Eq. [1]

$$i_h = k_h [H_3O^+]^{1/2} \exp[-\delta d] \exp\left[\frac{-\beta FE}{RT}\right] \qquad [2]$$

where subscript h denotes the high-cd region. The preexponential term k_h depends on the choice of a pH independent reference electrode against which E is given. It contains the factor for the dependence of the rates on oxygen partial pressure, which is first order, as well as other factors commonly encountered in an electrochemical rate